

# A Simulation of Three Dimensional Shaking Table Tests on a Full-Scale Four-Story Reinforced Concrete Building



**Yihuan Liu & Hitoshi Shiohara**  
*The University of Tokyo, Japan*

**Takuya Nagae & Taizo Matsumori**  
*National Research Institute for Earth Science and Disaster Prevention, Japan*

**SUMMARY:**

A full-scale four-story reinforced concrete wall-frame building specimen was tested on a three dimensional shaking table at E-Defense in Miki, Japan. In this paper, seismic responses predicted by a pretest computational simulation are compared with the measured test results, and the reliability of the state-of-the-art modeling methodology is evaluated. The test specimen was modeled based on measured structural dimensions, configurations and material properties. In order to avoid the correlative adjustment of modeling parameters, the simulation was done before the release of test results.

*Keywords: Nonlinear Dynamic Analysis, E-defense, Three Dimensional Shaking Table*

**1. GENERAL INSTRUCTIONS**

Nonlinear analysis has been growingly adopted as a useful tool for both seismic design and research. The adequacy of the constituent member models are usually investigated by static tests of small scaled models of structural members. However, the adequacy of damping, loading rate effect, and the other assumptions for modeling simplicity in frame analyses could not be verified by such static tests. Full scale three dimensional shaking table tests are the ultimate and only solution to overcome this challenge. National Research Institute for Earth Science and Disaster Prevention in Japan has conducted such three dimensional shaking table tests in the past, which includes a recent test of a full-scale four-story reinforced concrete building in December 2010 (Nagae et. al. 2011). The tests provide a benchmark for evaluating the state-of-art simulation technique. In this paper, the results of the simulation are compared with the experimental results.

**2. OUTLINE OF TEST PROGRAM**

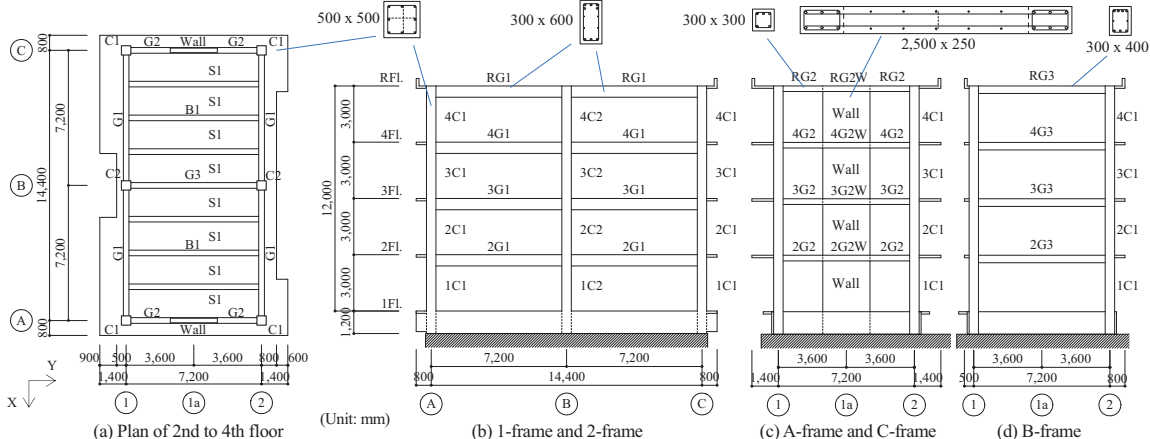


**Figure 1.** Plan and elevation of test specimen

A full-scale four-story reinforced concrete wall-frame structure specimen, designed and constructed in accordance with the Japanese seismic code and normal practice in Japan and the US, was tested at E-defense, Hyogo Earthquake Engineering Research Center in Miki, Japan. The total height of the building from the first floor level is 12.0 m. The floor plan is a rectangle of 7.2m by 14.4m. In X (longitudinal) direction, the building consists of two frames with two bays, while the Y (transverse) direction consists of two wall frames which are placed on the both sides of the building and a moment frame in the middle. The geometry of the building is presented in **Figure 1**. The specimen was sequentially subjected to six simulated base motions of JMA Kobe 1995 (amplified to 10%, 25%, 50% and 100% of the original record) then Takatori Kobe 1995 (amplified to 40% and 60% of the original record).

### 3. MODELING OF TEST SPECIMEN

OpenSees (OpenSees 2000) was used as the platform for the nonlinear dynamic analyses and static pushover analyses.

#### 3.1. General

Flexural dominant members such as columns and girders were modeled as single elements with fiber sections at the two ends, which is relatively simple and straight forward in preparing input data. For the modeling of shear walls, multiple elements were used. The modeling of columns, girders slabs, walls and joints in detail are to be discussed in the subsequent sections.

The mass of the building was discretized into floor masses and assigned to nodes intersected by beam and column. Lumped nodal masses were assumed to be identical in three translational directions. Rotational masses were not considered in any direction.

Rigid floor diaphragm was assumed for reducing the number of the translational DOFs in the lateral direction. The flexural capacity of the fiber model was found to be sensitive to the constraints (Liu Yihuan et. al. 2011). The rigid diaphragm constrains the expansion of fiber section and the flexural capacity of the beam increases. In order to avoid the overstrength, the axial stiffness of the mid part of every girder was set to be negligibly small by reducing the cross section area.

Damping matrix was assumed to be proportional to instantaneous stiffness matrix. Damping factors was taken as 1% for the first and third vibration mode, as no radiational damping was expected. Damping matrix was updated at each time step based on the updated stiffness matrix.

#### 3.2. Material

Uniaxial stress-strain relationships for steel and concrete were adopted in the simulation. All the global hysteretic behavior was represented based on uniaxial stress-strain relationship of individual fibers discretized in element sections (Spacone et. al. 1996). The effect of stirrup was considered indirectly by increasing strength and deformation capacity of concrete in confined zone. In OpenSees, various types of uniaxial stress-strain model are provided for steel and concrete. Material tagged “steel02” (OpenSees 2000, Menegotto et. al. 1995) and “concrete01” (OpenSees 2000, Kent et. al. 1973, Scott et. al. 1982) were used to represent reinforcing bars and concrete respectively, as shown in **Figure 2(b)**. The “concrete01” ignores tensile strength of concrete. One of the reasons why tensile strength was not considered here is that overestimation of yield strength and post-cracking stiffness was observed by a large number of RC flexural member tests. In order to achieve analytical convergence of a large scale model, the descending slope of tension softening of concrete needs to be limited under a less steep level, which causes overestimate of both strength and stiffness. Another reason is that the effective stiffness of a component shall correspond to the secant value to the yield point of the component according to FEMA 356. Without considering tension of concrete exactly

meets the requirements prescribed in FEMA 356. The parameters for unconfined and confined concrete model are summarized in **Table 1**.

**Table 1.** Parameters for unconfined and confined concrete model used in RC structure  
(Reference: [○] Mander et. al. 1988, [△] Paulay et. al. 1992)

	$f_c$	$\varepsilon_c$	$f_{cu}$	$\varepsilon_{cu}$	E
Unconfined	$f_c$	0.002	$0.2f_c$	0.004 [△]	$4700\sqrt{f_c}$ [△]
Confined	$f_{cc}$ [○]	$0.002[1 + 5(\frac{f_{cc}}{f_c} - 1)]$ [△]	$0.2f_{cc}$	$0.004 + \frac{1.4\rho_s f_y h \varepsilon_{sm}}{f_{cc}}$ [△]	

### 3.3. Modeling of Columns

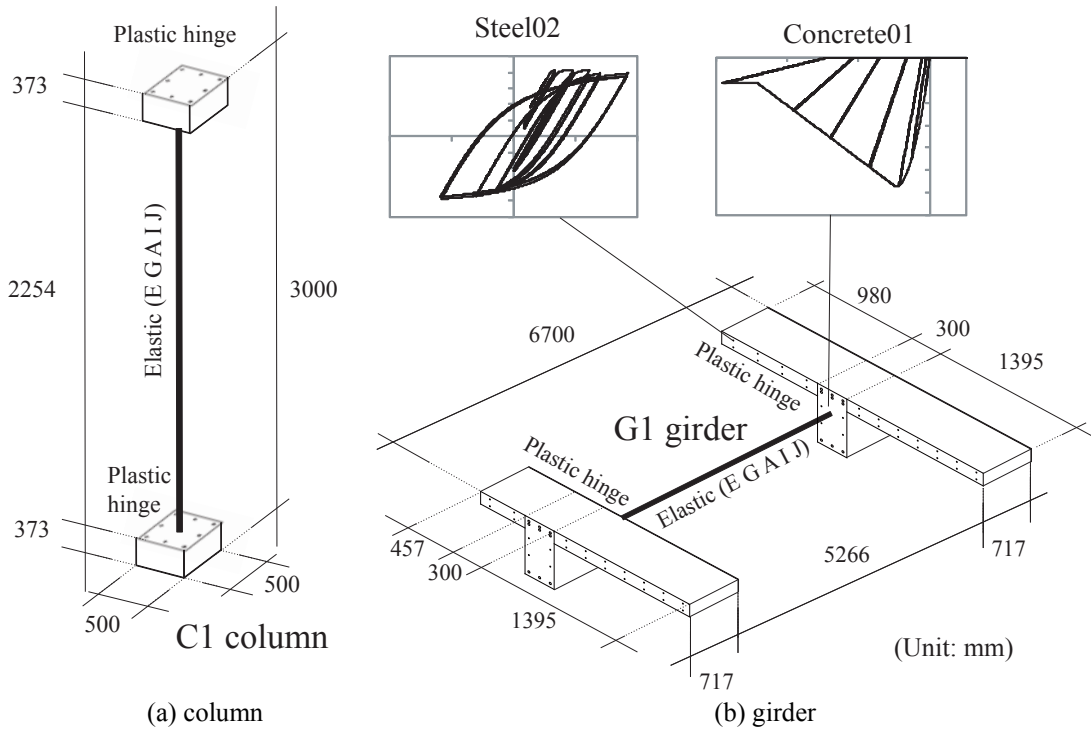


**Figure 2.** Fiber model

Columns were modeled by “beamWithHinges” element, which consists of two fiber sections at two ends and a linear elastic bar in the middle (**Figure 2(a)**, note that the strict formulation is somewhat different and it shall be referred to Michael et. al. 2006). Each element’s fiber section has uniaxial stress-strain relationship of different materials. Steel fibers are placed at the actual location of longitudinal reinforcement in a section. The concrete enclosed by stirrups was considered to be confined concrete. The cover concrete as well as slab concrete were considered to be unconfined concrete. Plastic hinge length  $l_p$  was calculated as  $l_p = 0.08L + 0.022f_y d_b$  (Paulay et. al. 1992), where  $l_p$  is the plastic hinge length,  $L$  is the column length,  $f_y$  is the yield strength of longitudinal reinforcements and  $d_b$  is the diameter of longitudinal reinforcements. Mechanical properties (elastic modulus, shear modulus, cross section area, moment of inertia and torsion constant) of the linearly elastic bars were calculated based on the gross concrete section, ignoring the contribution of reinforcements. “PDelta” command was used for geometrical transformation of column members in order to consider P-delta effect.

### 3.4. Modeling of Girders

The test specimen has three types of girders with different sections and they were modeled by “beamWithHinges” elements as shown in **Figure 2(b)** (Michael et. al. 2006). The difference to the modeling of columns is that the effect of slab was also taken into account. Each girder section was

modeled as a “T” section. Effective slab width was determined in accordance with AIJ Standard (AIJ 2010) (G1 girder of 457mm, 980mm and 1395mm, G2 girder of 420mm and G3 girder of 1340mm). Plastic hinge length was also taken as  $l_p = 0.08L + 0.022f_yd_b$  (Paulay et. al. 1992). Mechanical properties (elastic modulus, shear modulus, cross section area, moment of inertia and torsion constant) of the linear elastic bar were calculated based on gross concrete section, ignoring the contribution of reinforcements. Torsion constant was calculated based on the rectangular girder section excluding the slab. Note that axial stiffness was assumed to be negligibly small by reducing the cross section area in order to avoid the overstrength caused by rigid floor diaphragm (Liu Yihuan et. al. 2011).

**3.5. Modeling of Shear Walls**

Shear walls were modeled by Multiple-Vertical-Line-Element-Model (MVLEM) (Vulcano et. al. 1988). This model consists of three parts: multiple vertical trusses, a shear spring and multiple rigid elements as shown in **Figure 3**. The multiple vertical trusses represent the axial and flexural behavior, whereas the shear spring represents the shear behavior of the wall. Here, a wall section was divided into four smaller sections. In other words, a wall was divided into four columns. These columns are pinned on the ends in in-plane direction to represent the multiple vertical trusses in MVLEM, while fixed on the ends in out-of-plane direction to represent out-of-plane flexural behavior of wall. These vertical columns were modeled by “nonlinearBeamColumn” elements. The distributions of concrete and steel fibers in the vertical columns are based on the actual configurations of wall section as shown in **Figure 3**. The upper part and the lower part are connected with a zero-length elastic shear spring which has a horizontal translational stiffness. The stiffness was set to be linearly elastic and the value was taken as the initial shear stiffness ( $K = G_cA_{wall}/L_{wall}$ , based on gross concrete) of wall. Initially, the shear spring was assumed to be nonlinear (origin-oriented hysteresis) and the envelope obtained by monotonic loading was calculated based on Modified Compression Field Theory (Vecchio et. al. 1986). However, after the whole series of analyses, the maximum deformation was found not exceeding the cracking point. Therefore the shear spring was later set to be linearly elastic. The distance between the shear spring and the base is represented by parameter c. A suitable value of c is approximated based on the expected curvature distribution along the element height h. The value for c of 0.4 recommended by (Vulcano et. al. 1988) was used. Three stacks of the MVLEM unit were used in a story as shown in **Figure 4**.

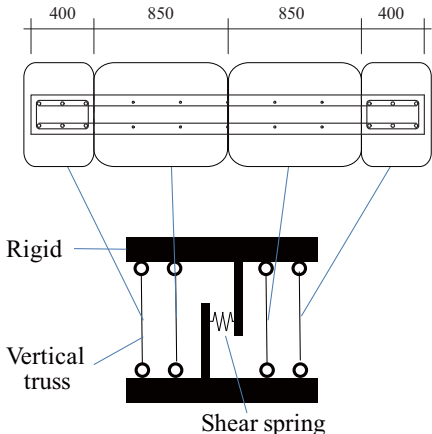


**Figure 3.** Multiple Vertical Line Element Model

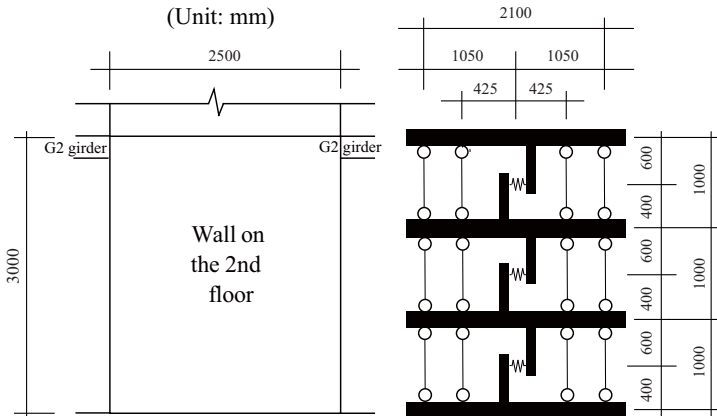


**Figure 4.** Multiple stacks

**3.6. Modeling of Beam-Column Joints**

Beam-column joints were modeled as rigid elements. Element tagged “elasticBeamColumn” was used to represent the rigid elements. The axial, flexural, shear, torsion stiffness of these elements was set to be much larger than the adjacent members.

## 4. PUSHOVER ANALYSIS

Base shear strength ratio reaches about 0.5 in X direction and 0.43 in Y direction respectively, as shown in **Figure 5**. Lateral load was applied with a vertical distribution of the product of story masses and first mode shape factors [Chopra 2000] (In X direction of  $m_n \phi_n = [0.08, 0.2, 0.32, 0.39]$  and in Y direction of  $m_n \phi_n = [0.06, 0.18, 0.32, 0.45]$ ).

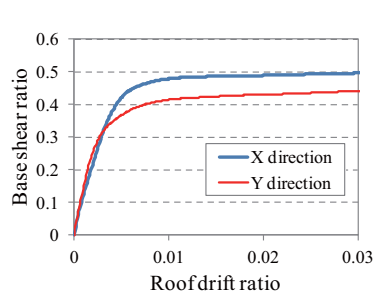
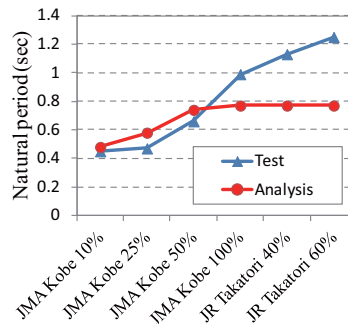
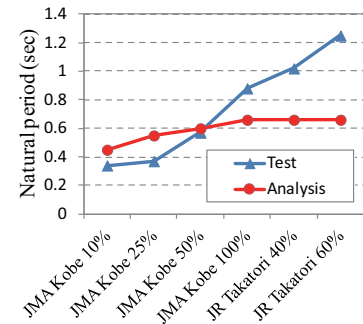


**Figure 5.** Pushover analysis



(a) X direction



(b) Y direction

**Figure 6.** Post-quake natural period

## 5. NONLINEAR DYNAMIC ANALYSIS

Nonlinear dynamic analyses were carried out with six ground motions, JMA Kobe 10%, JMA Kobe 25%, JMA Kobe 50%, JMA Kobe 100%, Takatori 40% and Takatori 60%, sequentially. Note that these input ground motions are the first floor accelerations measured on the shaking table during the tests. The sampling rate of the record was 200Hz, which corresponds to the size of a time step of numerical integration. Newmark's average acceleration method was used.

### 5.1. The Change in Natural Period

The post-Kobe 10% natural periods obtained by the test were 0.45 and 0.34 second in X and Y direction respectively (**Figure 6**). The calculated periods were 0.48 and 0.45 second, which overestimate 6.7% and 32% in X and Y direction respectively. The experimental natural period elongates significantly after each ground motion. However, analytical natural period stops elongating after Kobe 100% was applied, in both directions. In other words, the post-earthquake periods of Kobe 100%, Takatori 40% and 60% are the same. The discrepancy is probably due to the incapability of considering beam-column joint damage and wall base slip, which were actually observed during the tests. The natural periods of the test specimen above were determined by transfer functions subjected to white noise vibration (maximum amplitude of approximately  $0.3\text{m/s}^2$ ) after each strong ground motion. The natural periods of the analytical model were calculated by eigen analysis based on the post strong ground motion tangent stiffness matrix.

### 5.2. Initial Lateral Stiffness

The lateral stiffness is taken as the ratio of base shear force and first story inter-story drift ratio. Initial lateral stiffness can be compared when JMA Kobe 10% was applied. The vibration caused by JMA Kobe 10% is small and the building stays in elastic range both for test and analysis (**Figure 7**(a)). In X direction, the measured ( $220\text{kN/mm}$ ) and predicted initial lateral stiffness ( $209\text{kN/mm}$ ) are in very good agreement. In Y direction, the measured stiffness ( $593\text{kN/mm}$ ) is over 2 times larger than the analytical one ( $269\text{kN/mm}$ ). The underestimate might be caused by the neglect of small beams which support the floor slab in the analytical model. The reason for the speculation is explained as follows. During JMA Kobe 10%, the predicted longitudinal reinforcement strains in plastic hinge zone of G2 girders, which are parallel to the small beams, are significantly larger than the measured ones. During JMA Kobe 25%, it is estimated by analysis that some of the G2 girders begin to yield while none of the G2

girders actually yield according to the test results (indirectly reflected in **Figure 7(b)**). It indicates that the lateral strength was underestimated and the deficiency in strength might be due to the neglect of small beams which are parallel with G2 girders. Along with the underestimate of strength, stiffness is also underestimated.

### 5.3. Base Shear and the First Story Drift Ratio

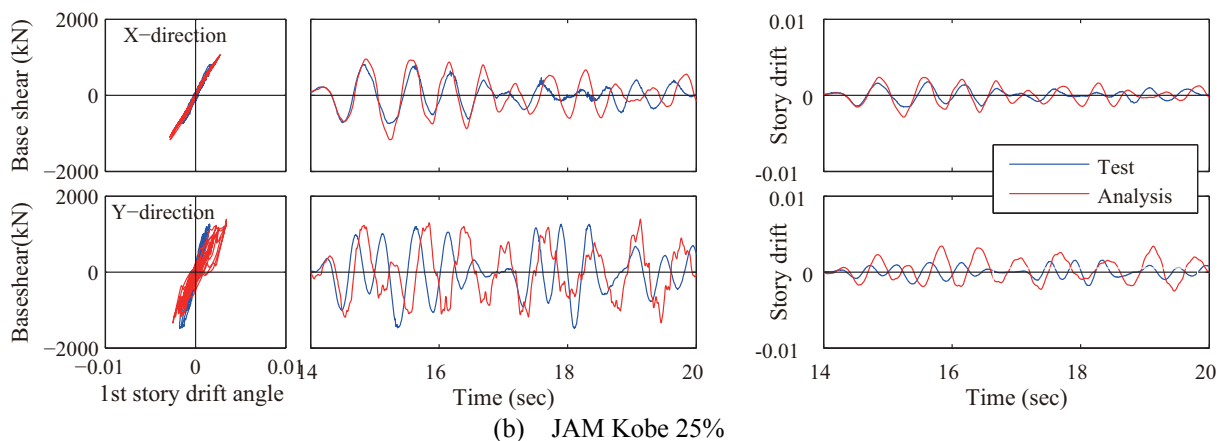
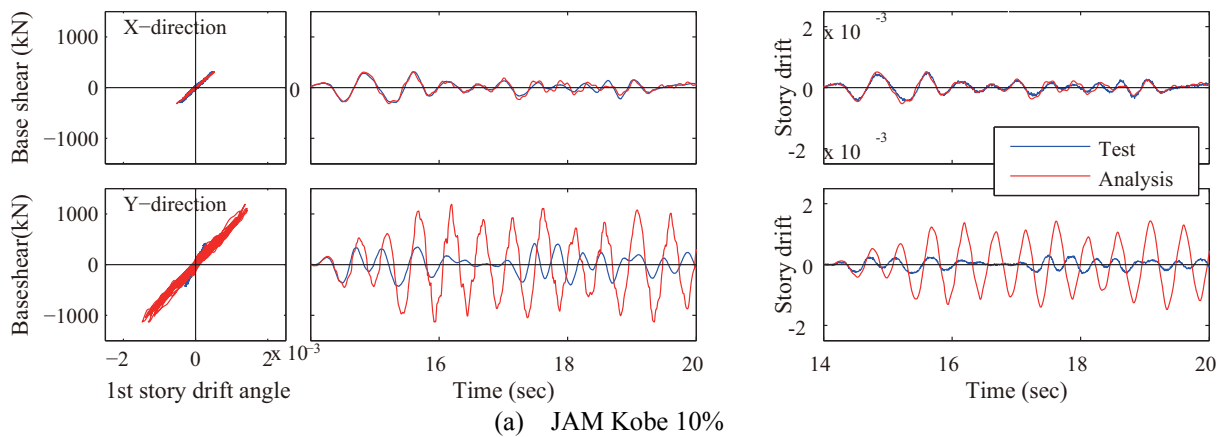
Most of the damage concentrates in the lower stories, especially at the first story, according to the test results. Therefore, the base shear and the first story drift ratio are presented in **Figure 7** and discussed as follows.

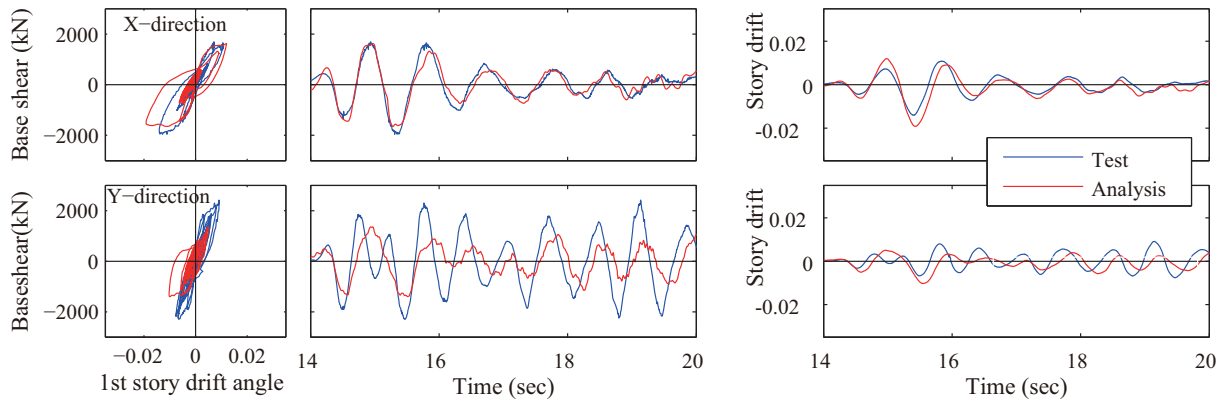
#### 5.3.1. Lateral strength

A large number of members yielded and the building reached its maximum lateral strength during the JMA Kobe 100% test (**Figure 7(d)**). In X direction, the analysis slightly underestimates the maximum base shear (about 19%). In Y direction, the analysis underestimates significantly (about 46%). Note that the measured strength is also significantly larger than the design strength according to the test (Nagae et. al. 2011). The reason for the overstrength is still under investigation.

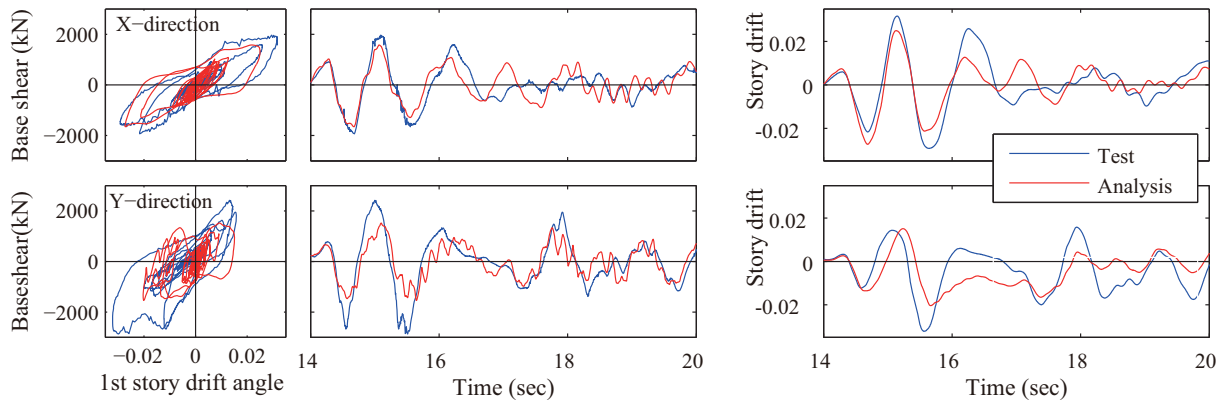
#### 5.3.2. X direction

Both base shear and story drift obtained by the tests and the analyses are in very good agreement when the pre-quake damage state is relatively low (from JMA Kobe10% through JMA Kobe100% as seen in **Figure 7(a)(b)(c)(d)**). The analytical and experimental hysteresis loops are also similar in shape (**Figure 7(c)(d)**). When the pre-quake damage state is high (JR Takatori 40% and 60% as seen in **Figure 7(e)(f)**), the measured lateral stiffness deteriorates significantly. Energy dissipation capacity also degrades with pinched hysteretic behavior. While for analysis, the lateral stiffness does not deteriorate at all during these two ground motions and no elongation of the natural period was observed after these quakes (**Figure 6**).

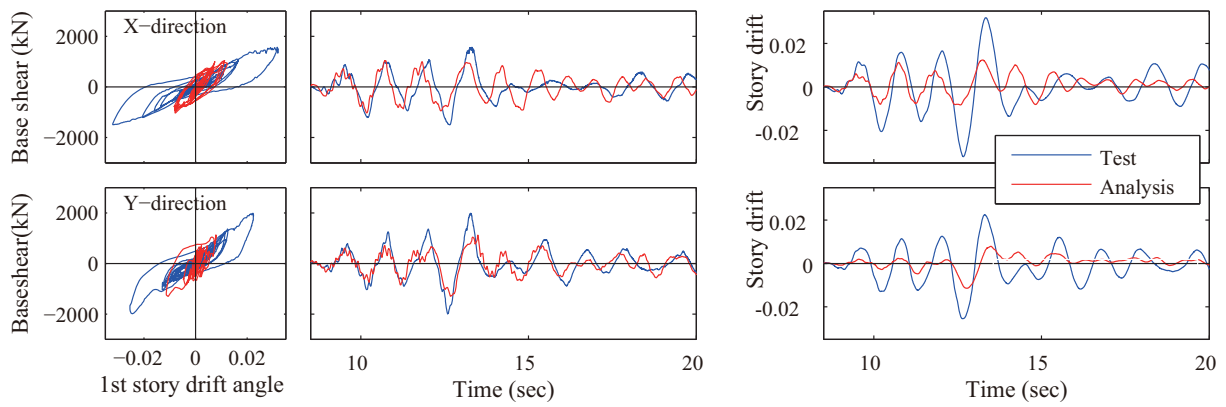




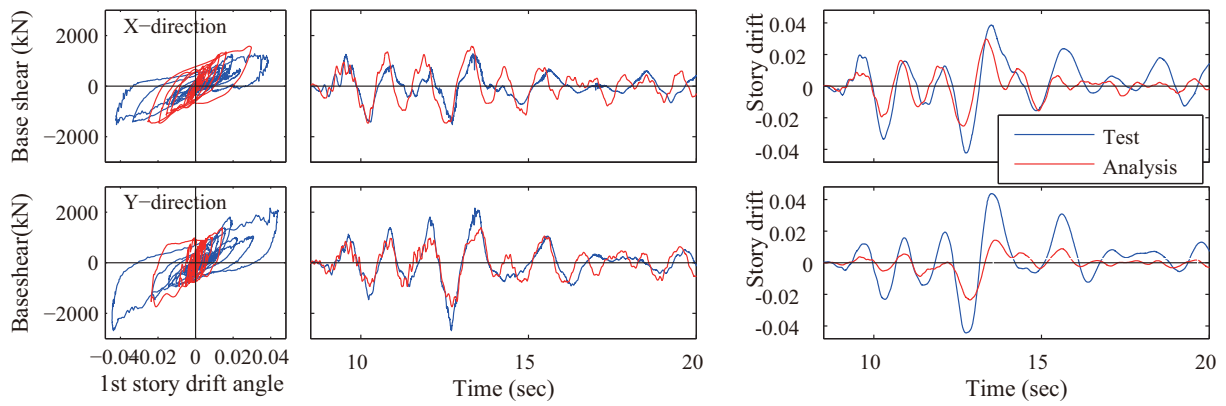
(c) JAM Kobe 50%



(d) JAM Kobe 100%



(e) JR Takatori 40%



(f) JR Takatori 60%

**Figure 7.** Base shear, first story drift ratio and hysteresis

The hysteresis obtained by the analysis shows large hysteretic loops without any pinch. Furthermore, for the last two ground motions, the measured story drift is significantly larger than that of the analysis. The discrepancy is probably due to the neglect of the nonlinear behavior of beam-column joints in the analytical model. According to the test report (Nagae et. al. 2011), story drift due to the deformation of the beam-column joints was found to be extraordinarily large, reaching over 60% and 80% of the total story drift for JR Takatori 40% and 60% ground motion respectively.

### 5.3.3. Y direction

For the low pre-quake damage states (from JMA Kobe10% to JMA Kobe50%, **Figure 7(a)(b)(c)**), experimental and analytical results of both base shear and story drift are significantly different in either phase or amplitude. The discrepancy was caused by the difference in the natural periods, which may be originally caused by the neglect of the small beams in the analytical model. For the high pre-quake damage states (from JMA Kobe100% to JR Takatori60%, **Figure 7(d)(e)(f)**), the analyses tend to have better estimation of the phase of the time-dependent base shear. However, the amplitude of the time-dependent base shear is considerably underestimated and of story drift largely underestimated (**Figure 7(d)(e)(f)**). The energy dissipation capacity of the analytical model appears to be slightly larger than that of the test specimen (**Figure 7(e)(f)**). The possible reason for the significant underestimation of the deformation is that the analytical model does not consider the slip at wall base, which in fact occurred during the tests. During the tests, severe slip along the wall base at the first floor was observed and the slip contributes over 40% of the total first floor inter-story drift during JMA Kobe 100% (Nagae et. al. 2011).

## 5.4. Maximum Story Drift Ratios

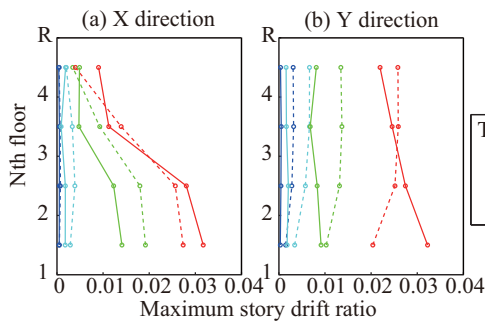


**Figure 8.** Maximum Story drift ratio

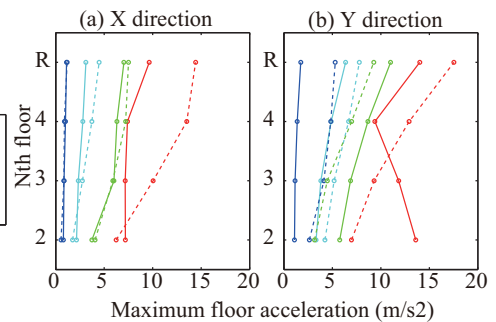


**Figure 9.** Maximum floor acceleration

### 5.4.1. X direction

The analytical and the experimental results give similar profiles of vertical distributions of the maximum story drifts (**Figure 8(a)**), which indicate that the yielding mechanisms are in good agreement. While the magnitude of the story drifts for JMA Kobe 25% and 50% is considerably overestimated (61% and 36% for the first floor respectively). The difference in period may be one of the reasons that cause the discrepancy.

### 5.4.2. Y direction

The analytical results overestimates the story drifts notably for the upper stories (**Figure 8(b)**). This is probably due to the difference in the natural period. In the first story, analyses overestimate significantly for JMA Kobe 10% and 25%. But the overestimate decreases rapidly for JMA Kobe 50% and subsequently turns into significant underestimate for JMA Kobe 100%. The probable reason is that during JMA Kobe 100% test, first floor wall base began to slip severely. The slip actually contributes a large percentage of total story drift while the analytical model cannot consider this additional deformation and therefore causes large underestimate for JMA Kobe 100%.

## 5.5. Maximum Floor Acceleration

Generally, the profiles of vertical distribution of maximum floor accelerations are well estimated for relatively weak ground motions (JMA Kobe 10%, 25% and 50%) while very poorly estimated for

JMA Kobe 100% (see **Figure 9**).

### 5.6. Maximum Strain of Longitudinal Reinforcements and Plastic Hinge Distributions

Plastic hinge distributions obtained by the tests and the analyses after applying JMA Kobe 50% are similar in pattern as shown in **Figure 10**, which indicates that the yielding mechanism in X direction is well captured by the analyses. The maximum strains of longitudinal reinforcements are also in good agreement as shown in **Figure 10**. Strains of the longitudinal reinforcements were measured by strain gauges which were attached to the longitudinal reinforcements located at the plastic hinge zones. For both of the test and the analysis, a plastic hinge is assumed to form when the maximum strain in the plastic hinge zone reaches a value of 0.0018 (both of the longitudinal reinforcements in columns and girders are D22 reinforcing bars in frame direction). In **Figure 10**, the area of the circles represents the magnitude of maximum strains and the black circles indicate that any of the maximum strains within the plastic hinge zone exceeds yield strain. Except for the plastic hinge zones in the second floor girder and the exterior joint zone on the third floor, the errors of the predicted maximum strains do not exceed 85%. The prediction of local damage is considered to be fairly accurate for a macroscopic model.

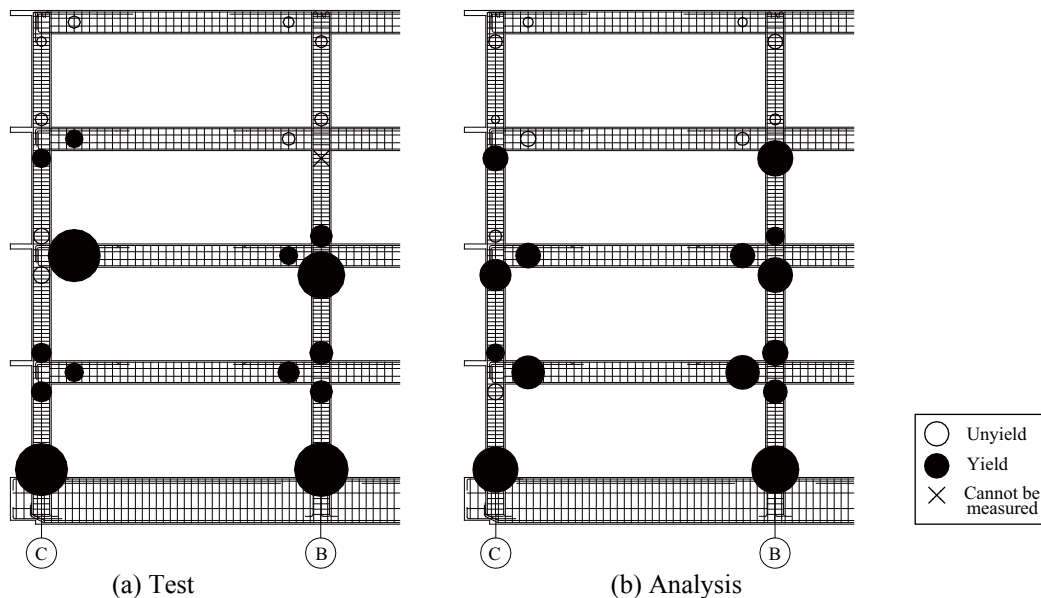


**Figure 10.** Maximum strains of longitudinal reinforcements and plastic hinge distributions in frame direction (JMA Kobe 50%)

## 6. CONCLUDING REMARKS

The simulation of a series of shaking table tests of a full-scale four-story reinforced concrete building with the state-of-art modeling technique is reported. The major findings of this study are summarized as follows:

### (1) Yielding mechanism and deformation

Yielding mechanism is well captured with major damage concentrated in the lower stories for the frame direction. For relatively low pre-quake damage state (JMA Kobe 10%, 25%, 50%, 100%), story drifts are well estimated. For relatively large pre-quake damage state (JR Takatori 40%, 60%), story drifts are generally significantly underestimated.

For relatively low pre-quake damage state (JMA Kobe 10%, 25%, 50%), the natural period is considerably overestimated, causing large overestimate of story drifts for the wall direction. For relatively large pre-quake damage state (JMA Kobe 100%, JR Takatori 40%, 60%), the estimated yielding mechanism greatly differs from the measured one. The simulation fails to reproduce the

mechanism that damage concentrates in the first story.

### (2) Lateral strength

The lateral strength is acceptably well predicted in frame direction, while notably underestimated in wall direction.

### (3) Natural period

For relatively low pre-quake damage state (JMA Kobe 10%, 25%, 50%, 100%), the analytical model is able to track the elongation of period due to damage evolution. However, for relatively large pre-quake damage state (JR Takatori 40%, 60%), the elongation of period stops.

## ACKNOWLEDGEMENT

The authors thank National Research Institute for Earth Science and Disaster Prevention, Japan for conducting the shaking table test and sharing test data.

## REFERENCES

- Architectural Institute of Japan, (2010), AIJ Standard for Structural Calculation of Reinforced Concrete Structures -Based on Allowable Stress Concept-
- Chopra, Anil K., (2000) Dynamics of Structures: Theory and Applications to Earthquake Engineering, Prentice-Hall
- Kent, D. C. and Park, R., (1971), Flexural Member with Confined Concrete, *Journal of the Structural Division*, ASCE, **Vol. 97**, 1969-1990
- Liu Yihuan, Shiohara Hitoshi, (2011), Overstrength Effect of Axial Constraint to Fiber Section Beam Column Element, *Japan Architecture Conference Synopsis collection*, **Vol. 2011**, 289-290
- Mander, J.B., Priestley, M.J.N, Park, R., (1988), Theoretical stress-strain model for confined concrete, *Journal of Structural Engineering*, ASCE, **Vol.114**, No. 8, pp. 1804-1825.
- Menegotto, M. Pinto, P.E., (1973), Method of analysis of cyclically loaded RC plane frames including changes in geometry and non-elastic behavior of elements under normal force and bending, Preliminary Report, IABSE, **Vol. 13**, pp. 15–22.
- Michael H. Scott, Gregory L. Fenves, (2006), Plastic Hinge Integration Methods for Force-Based Beam — Column Elements, *Journal of Structural Engineering*, **Vol. 132**, No. 2., pp. 244-252
- OpenSees Development Team, (2000), Open system for earthquake engineering simulation (OpenSees), Pacific Earthquake Engineering Research Center, University of California, Berkeley, California, U.S.A., <http://opensees.berkeley.edu/>.
- Paulay, T., Priestley, M.J.N., (1992), Seismic Design of Reinforced Concrete and Masonry Buildings, John Wiley & Sons, Inc., pp. 98-103.
- Scott, B.D., Park, R., Priestley, M.J.N., (1982), Stress-Strain Behavior of Concrete Confined by Overlapping Hoops at Low and High Strain Rates, *Journal of the American Concrete Institute*, **Vol 79**, **Issue 1**, Pages 13-27
- Spacone, E. Filippou, F.C., Taucer F., (1996), Fiber Beam-Column Model for Nonlinear Analysis of R/C Frames: I. Formulation, *International Journal of Earthquake Engineering and Structural Dynamics*, **Vol. 25**, No. 7, pp. 711-725.
- Takuya Nagae, Kenichi Tahara, Kunio Fukuyama, Taizo Matsumori, Hitoshi Shiohara, Toshimi Kabeyasawa, Susumu Kono, Minehiro Nishiyama, Isao Nishiyama, (2011), Large-scale Shaking Table Tests on a Four-story RC Building, *Journal of Structural and Construction Engineering*, AIJ, **Vol. 76**, No. 669, 1961-1970, (in Japanese).
- Vecchio, F. J. and Collins, M. P., (1986), The modified compression field theory for reinforced concrete elements subjected to shear, *ACI Structural Journal*, **Vol. 83(2)**, pp. 219-231
- Vulcano A, Bertero VV, Colotti V., (1988), Analytical modeling of RC structural walls, *Proceedings, 9th world conference on earthquake engineering*. **Vol. 6**.1988. p. 41-6.